Efficient synthesis of phycocyanobilin in mammalian cells for optogenetic control of cell signalings.

Youichi Uda[a,b], Yuhei Goto[b], Shigekazu Oda[b], Takayuki Kohchi[c], Michiyuki Matsuda[a,d], and Kazuhiro Aoki[b,e,f1]

[a] Department of Pathology and Biology of Diseases, Graduate School of Medicine, Kyoto University, Sakyo-ku, Kyoto 606-8501, Japan

[b] Division of Quantitative Biology, Okazaki Institute for Integrative Bioscience and National Institute for Basic Biology, National Institutes of Natural Sciences, Okazaki, Aichi 444-8787, Japan.

[c] Laboratory of Plant Molecular Biology, Graduate School of Biostudies, Kyoto University, Sakyo-ku, Kyoto 606-8502, Japan

[d] Laboratory of Bioimaging and Cell Signaling, Graduate School of Biostudies, Kyoto University, Sakyo-ku, Kyoto 606-8501, Japan

[e] Imaging Platform for Spatio-Temporal Information, Graduate School of Medicine, Kyoto University, Sakyo-ku, Kyoto 606-8501, Japan

[f] Department of Basic Biology, Faculty of Life Science, SOKENDAI (Graduate University for Advanced Studies), Myodaiji, Okazaki, Aichi 444-8787, Japan;

[1] To whom correspondence may be addressed. Email: k-aoki@nibb.ac.jp

Short title: Genetically-encoded phytochrome B-PIF LID system

Classification: BIOLOGICAL SCIENCE

Key words: Optogenetics, cell signaling, phytochrome

Final publication is available at http://www.pnas.org/content/114/45/11962

Abstract

Optogenetics is a powerful tool to precisely manipulate cell signaling in space and time. For example, protein activity can be regulated by several light-induced dimerization (LID) systems. Among them, the phytochrome B (PhyB)-phytochrome-interacting factor (PIF) system is the only available LID system controlled by red and far-red lights. However, the PhyB-PIF system requires phycocyanobilin (PCB) or phytochromobilin as a chromophore, which must be artificially added to mammalian cells. Here, we report an expression vector that expresses four enzymes for the efficient synthesis of PCB in the mitochondria of mammalian cells. An even higher intracellular PCB concentration was achieved by the depletion of biliverdin reductase A, which degrades PCB. The PCB synthesis and PhyB-PIF systems allowed us to optogenetically regulate intracellular signaling without any external supply of chromophores. Thus, we have provided a practical method for developing a fully genetically-encoded PhyB-PIF system, which paves the way for its application to a living animal.

Significance Statement

Optical control of cell signaling has attracted much attention in recent years. Most optogenetic systems exploit blue light as do fluorescent indicators such as FRET-based biosensors. Phytochrome B (PhyB)-phytochrome interacting factor (PIF) is a red/far-red light-switchable heterodimerization system. However, PhyB requires phytochromobilin or phycocyanobilin (PCB) as a chromophore, which must be externally added to mammalian cells. To overcome this difficulty, we developed a system for an efficient synthesis of PCB in mammalian cells. Eventually, we found that PCB was synthesized by introducing all *PcyA*, *HO1*, *Fd* and *Fnr* genes. The knockout or knockdown of *biliverdin reductase A* further enhanced PCB synthesis. This genetically-encoded PCB synthesis system allowed us to manipulate cell signaling by red/far-red light without exogenous PCB addition.

Introduction

Intracellular signal transduction pathways are information-processing systems in which the information of input signals is processed, and subsequently leads to the generation of output responses as cellular phenotypes (1, 2). These pathways are comprised of a series of biochemical reactions with cross-talk regulations and feedback regulations that form a highly complex network (3–5). While the complexity of the intracellular signaling network poses a significant challenge, considerable evidence has accumulated that certain network modules such as feedback loops have developed an intrinsic resistance to molecular targeted drugs (6–8), highlighting the critical importance of understanding the signaling network as a system.

Methods capable of rapidly and reversibly perturbing cellular systems are essential for analyzing the dynamics of feedback and cross-talk regulations. The perturbations have to be faster than the representative time constant of a feedback regulation to track the transient change in the system (9). While a chemical-induced dimerization (CID) system has been widely used to quickly perturb cellular signaling by small compounds (10), most CID systems are irreversible, and it is difficult to manipulate the dimerization at the subcellular level. Currently, several light-induced dimerization (LID) systems, in which photoactivatable proteins are dimerized by light in a reversible manner, are available. Among them, the cryptochrome 2 (CRY2) and cryptochrome-interacting basic helix-loop-helix1 (CIB1) pair has been widely used to control cell signaling through its light-induced heterodimerization (11–13). The CRY2 associates with its binding partner CIB1 upon exposure to blue light within few seconds, and the complex is dissociated under a dark condition within several minutes (14). The CRY2 protein utilizes flavin as a chromophore, and the CRY2-CIB1 LID system is thereby fully genetically-encoded, so that it is not necessary to add a cofactor to mammalian cells. However, this system has potential drawbacks. First, the dissociation reaction has slow kinetics and is uncontrollable, though faster dissociation mutants of the CRY2-CIB1 pair have been reported recently (15). Second, the use of blue light for photoactivation of the CRY2-CIB1 is not compatible with fluorescence imaging with GFP-based biosensors such as FRET biosensors (16, 17).

Currently, Phytochrome B (PhyB) – Phytochrome Interacting Factor (PIF) is

the only LID system that operates at long wavelength light (14, 18, 19). PhyB ligates phycocyanobilin (PCB) or phytochromobilin as a photoabsorbing chromophore (20). Upon red light exposure, PhyB binds to PIF within seconds, and the resulting PhyB-PIF complex dissociates within seconds upon far-red light exposure. Taking advantage of its potential for quick and reversible control of association and dissociation by light, researchers have used the PhyB-PIF system to manipulate cellular signaling at higher resolution in both space and time (14, 18, 21). However, there is also a key disadvantage of the PhyB-PIF system. Namely, the chromophore is produced only in photosynthetic organisms; in other organisms, the chromophore must be added before the PhyB-PIF system can be applied. To overcome this issue, a PCB biosynthesis system has been constructed in bacterial and mammalian cells by expressing two biosynthetic enzymes, heme oxygenase1 (HO1) and PCB:ferredoxin oxidoreductase (PcyA) (Fig.1A) (22–24). So far, however, no PCB biosynthesis system has been used successfully to operate the PhyB-PIF system in mammalian cells, probably because the biosynthesis systems tested did not yield sufficient amounts of PCB for the PhyB-PIF system (Fig. 1A).

In this study, we demonstrate that PCB biosynthesis in mammalian cells is enormously boosted by the co-expression of *Ferredoxin* (*Fd*) and *Ferredoxin-NADP*$^+$ *reductase* (*Fnr*) with *HO1* and *PcyA*. A further increase in PCB synthesis is achieved by knock-out (KO) or knock-down (KD) of *biliverdin reductase A* (*BVRA*). Using this genetically-encoded PCB synthesis system, we have succeeded in optogenetic control of cell signaling by the PhyB-PIF system in the absence of exogenous chromophores.

Results

Reconstitution of the PCB synthesis pathway in mammalian cells

Two enzymes, heme oxygenase (25) and ferredoxin-dependent bilin reductase (26, 27), are committed to phytochrome chromophore biosynthesis from heme. In photosynthetic organisms such as cyanobacteria, PCB is produced from heme through HO1-mediated heme oxidation, followed by PcyA-mediated biliverdin reduction (Fig. 1A). Both reactions are coupled with a reduction of reduced Ferredoxin (Fd). The oxidized Fd (Fd_{ox}) is then reduced by Ferredoxin-NADP+ reductase (Fnr) to regenerate reduced Fd. In our preliminary experiments, expression of HO1 and PcyA derived from

Thermosynechococcus elongatus BP-1 was not sufficient for operation of the PhyB-PIF system in mammalian cells. We hypothesized that the failure might have been due to the lack of Fd and Fnr. Because heme exists primarily at mitochondria in mammalian cells (28, 29), we attempted to co-express Fd and Fnr derived from *Synechocystis* sp. PCC6803
with HO1 and PcyA to reconstitute the PCB synthetic pathway in human cells.

To quantify the amount of PCB in a living cell, we employed the Tyr-276-His mutant of PhyB (PhyB-Y276H), which emits red fluorescence upon binding to PCB (30) (Fig. 1B). The PhyB-Y276H protein was fused with mCherry, which was used as an internal standard, and the H-Ras C-terminus (HRasCT) was used for plasma membrane localization. HeLa cells expressing PhyB-Y276H-mCherry-HRasCT emanated 680 nm red fluorescence in the presence of exogenous PCB (Fig. 1C). Müller *et al.* realized PCB synthesis in mammalian cells by using a pKM087 expression vector that encodes mitochondria-targeting sequence (MTS)-fused with PcyA and MTS-HO1 (31). However, the fluorescence from PhyB-Y276H was below the detectable level in pKM087-expressing HeLa cells (Fig.1C and D).

To our surprise, when MTS-Fd and MTS-Fnr were co-expressed with MTS-PcyA and MTS-HO1, the red fluorescence of PhyB-Y276H from HeLa cells became almost comparable to that observed in the presence of 2.5 μM PCB (Fig. 1C and D). Exclusion of any one of these four genes abolished the fluorescence from the cells (Fig. 1D). Human homolog of HO1, Fd, or Fnr was unable to substitute for HO1, Fd, or Fnr in PCB synthesis (Fig. S1). These data indicated that PcyA, HO1, Fd, and Fnr, which are derived from *Thermosynechococcus elongatus* BP-1 or *Synechocystis* sp. PCC6803*,* were required for the efficient PCB production in mammalian cells.
To facilitate gene delivery, these four genes were connected with the cDNA of self-cleaved P2A peptide, generating a synthetic gene “PHFF” (Fig. 1E and Fig. S2). The HeLa cells transfected with the pPHFF expression vector for PHFF emanated red fluorescence from PhyB-Y276H at a level comparable to those of cells expressing the four genes independently (Fig. 1F and G). PCB is known to be covalently attached to Phytochrome B. The covalent attachment of PCB to the PhyB was confirmed by SDS page followed by zinc blot analysis (Fig. S3). Moreover, PHFF-expressing *Schizosaccharomyces pombe* produced intracellular PCB to the level evoked by the

addition of saturating amount of extracellular PCB (Fig. S4 and Table S1).

LID by the PHFF-PhyB-PIF system

Next, we examined whether expression of pPHFF is sufficient for PhyB binding to PIF. For this purpose, PhyB-mCherry-HRasCT and PIF-mEGFP were co-expressed at the plasma membrane and cytosol, respectively, with pPHFF. The cells were reciprocally illuminated with red and far-red lights to turn on and off, respectively, the binding of PIF-mEGFP to PhyB-mCherry-HRasCT at the plasma membrane (Fig. 2A). We examined four pairs of PhyB and PIF, i.e., PhyB (1-908 a.a.) and PhyB621 (1-621 a.a.) for the PhyB's (Fig. 2B), and PIF3 and PIF6 for the PIF's (32). PhyB621 was comprised of the minimal photosensory core, namely the PAS-like, GAF and Phy domains (33). The pair of PhyB and PIF3 resulted in a clear change in PIF3 distribution upon red and far-red light exposure, whereas the pair of PhyB621 and PIF3 showed a limited subcellular relocalization (Fig. 2C and 2D, upper panels, Movie S1). PIF6 was also associated with PhyB and PhyB621 under the red light exposure, while it was not completely dissociated from PhyB and PhyB621 by the far-red light (Fig. 2C and D, lower panels, Movie S1). The reductions of cytoplasmic PIF-mEGFP intensities compared with the far-red light condition were quantified for each of these four combinations (Fig. 2D-G), indicating fast and reversible membrane translocation of PIF by red and far-red light exposure on the second time scale (Fig. 2D-G). Interestingly, PIF3 reproducibly showed faster association and dissociation rate constants than PIF6.

Enhancement of PhyB-PIF LID by the depletion of BVRA

To further enhance PhyB-PIF LID, we depleted biliverdin reductase A (BVRA), which metabolizes biliverdin and PCB into bilirubin and phycocyanorubin, respectively (34) (Fig. 3A). To this end, we established *BVRA* KO HeLa cells by using the CRISPR/Cas9 system. As expected, the KO of *BVRA* reduced intracellular bilirubin, as visualized by UnaG, a bilirubin sensor (35) (Fig. S5). In *BVRA* KO HeLa cells, PhyB-Y276H fluorescence was increased to approximately three-fold the level in control HeLa cells (Fig. 3B and C). RNAi-mediated KD of *BVRA* also increased PhyB-Y276H fluorescence (Fig. S6). The enhancement of PhyB-Y276H fluorescence may have been due to the decrease in degradation of PCB, because *BVRA* KO HeLa cells demonstrated

higher PCB fluorescence by the addition of purified PCB than control HeLa cells did (Fig. 3D). Meanwhile, it is reported that supplementation of Heme precursor, 5-aminolevulinic acid (ALA) and iron(ii) sulfate, increases Biliverdin biosynthesis up to three-fold (36). Contrary to our expectation, these treatments did not significantly increase PCB synthesis in either control HeLa or BVRA KO HeLa cells that expressed PHFF (Fig. S7). Notably, neither the expression of PHFF nor the depletion of BVRA affected cell growth rates in HeLa cells and mouse embryonic stem cells (mESCs) (Fig. S8).

Next, we evaluated the effect of *BVRA* KO on LID in the same PhyB and PIF pairs as in Figure 2A. In *BVRA* KO HeLa cells expressing PHFF, both the PIF3 and PhyB pair and PIF3 and PhyB621 pair showed distinct translocation of PIF3-mEGFP upon red light and far-red light exposure (Fig. 3E, upper panels, Movie S2). PIF6 also demonstrated clear association with PhyB and PhyB621 by red light exposure, but a substantial amount of PIF6-mEGFP remained at the plasma membrane even under a far-red light condition in both the combinations with PhyB and that with PhyB621 in *BVRA* KO HeLa cells (Fig. 3E, lower panels, Movie S2). The quantification showed a much better response of PIF-mEGFP translocation in *BVRA* KO cells (Fig. 3F-I) than control cells (Fig. 2D) under all conditions. The PIF3 and PhyB pair exhibited rapid translocation almost comparable to that of the PIF3 and PhyB621 pair, with reversible PIF translocation (Fig. 3F-I, upper panels). Meanwhile, slower and smaller translocations of PIF6-mEGFP were observed with the PIF6 and PhyB pair and PIF6 and PhyB621 pair, respectively (Fig. 3F-I, lower panels). On the other hand, we verified whether PhyB-PIF3 combination is effective in other types of cell. PCB synthesis was also observed in mESCs and mouse embryonic fibroblasts (MEFs) that expressed PHFF and shRNA against mouse *BVRA* (Fig. S6, S9). Under this condition, PhyB-PIF3 LID was reproducibly observed in mESCs (Fig. S9).

Application of the PhyB-PIF system to manipulating signal transduction

Finally, we employed the genetically-encoded PhyB-PIF system to control intracellular signaling. It is known that activation of Rac1, a small GTPase, leads to actin reorganization and lamellipodia formation (37). To optogenetically activate the endogenous Rac1 protein, Tiam1, a Rac1-specific guanine nucleotide exchange factor

(38) was fused with PIF3 and mEGFP, and this chimeric protein was recruited to the plasma membrane through binding to PhyB-mCherry-HRasCT upon exposure to red light (Fig. 4A). Indeed, red light exposure induced rapid formation of thin lamellipodia along the cell periphery in HEK-293 cells expressing sh-hBVRA (Fig. 4B and C, Movie S3), indicating the activation of Rac1 by light illumination.

One advantage of the PhyB-PIF system is that it enables both the manipulation of cell signaling and detection of the output signals with a GFP reporter or CFP/YFP-based FRET biosensor. The ERK MAP kinase pathway was activated by the recruitment of CRaf-PIF3 to the plasma membrane by red light, and the subsequent activation of ERK was monitored by EKAREV-NLS, an ERK FRET biosensor (39) (Fig. 4D). Importantly, the excitation light for the FRET biosensor caused slight PhyB activation, and therefore the non-specific activation was prevented by global illumination with far-red light. The FRET/CFP ratio, which correlated with ERK activity (11), was increased upon red light illumination (Fig. 4E and Movie S4), and this increase was suppressed by far-red light illumination (Fig. 4F).

Discussion

We induced PCB synthesis in mammalian cells through the expression of a synthetic gene, PHFF, that was made up of the four genes *PcyA*, *HO1*, *Fd* and *Fnr*, which are derived from *Thermosynechococcus elongatus* BP-1 or *Synechocystis* sp. PCC6803. Moreover, *BVRA* KO or *BVRA* KD was shown to increase the level of cellular PCB by reducing the metabolism of biliverdin and PCB (34). The amount of synthesized PCB was sufficient for use in a genetically-encoded PhyB-PIF system for the modulation of intracellular signaling.

Müller *et al.* have reported PCB synthesis by the expression of *HO1* and *PcyA* in mammalian cells (31), but we found that the amount of PCB synthesized by this method was not sufficient for operation of the PhyB-PIF system. Of note, mammalian cells endogenously express ferredoxin-1, an Fd-like protein (also known as adrenodoxin) (40). However, the amino-acid sequence homology between human ferredoxin-1 and *Synechocystis* sp. PCC 6803 Fd was limited to 26%. Additionally, sequence and structure studies of mammalian ferredoxin-NADP+

reductase/adrenodoxin reductase suggested no functional overlap with *Synechocystis* sp. PCC 6803 Fnr (41, 42). The robust increase in PhyB-Y276H fluorescence observed in the present study (Fig. 1C and D) strongly suggests that mammalian ferrodoxin-1/adrenodixin and ferredoxin-NADP+ reductase/adrenodoxin reductase cannot support the PCB synthesis by cyanobacterial *HO1* and *PcyA*.

Faster association and dissociation kinetics were observed in the PIF3-PhyB bindings in comparison to the PIF6-PhyB bindings (Figs. 2 and 3). PIF6 was originally reported to show fast and reversible bindings to PhyB in the LID system (18). However, under our experimental conditions, PIF6 tended to be retained at the plasma membrane even after far-red light exposure (Figs. 2 and 3). Although the precise mechanisms underlying this retention are still unclear, the sustained binding of PIF6 to PhyB may leak signals of the LID system even under far-red light illumination, and eventually decrease ON and OFF responses. For this reason, PIF3 would be more suitable than PIF6 as a binding partner of PhyB in the PhyB-PIF system.

Depletion of BVRA by CRISPR/Cas9-mediated gene KO or shRNA resulted in an enhancement of PCB synthesis, and thereby an increase in the efficiency of PhyB-PIF LID (Fig. 3 and Fig. S6). Heme and its metabolites, biliverdin and bilirubin, are known to have diverse physiological functions including electron transfer, anti-oxidant and cell signaling, respectively (28, 43, 44), though their cellular functions remain controversial (45). In our experiments, we did not observe any detectable effects of PHFF expression and/or *BVRA* KD on cell growth rates in HeLa cells and mESCs (Fig. S8). This might be because biliverdin and bilirubin are delivered from the serum. Additionally, it should be noted the possible alteration of insulin signaling by depletion of *BVRA* gene (46). Therefore, new strategies are needed to improve PCB synthesis without affecting BVRA function.

The genetically-encoded system of PCB synthesis will provide a potential advantage for establishing transgenic animals that stably synthesize PCB endogenously, thereby enabling the optogenetic manipulation of cell signaling in deeper tissues without injecting PCB. Biliverdin-bound PhyB mutants or other phytochromes should also be explored in future studies.

Materials and Methods

Plasmids

pKM087 was the kind gift of Dr. Weber (31). The cDNAs of *PcyA* and *HO1*, which were originally derived from *Thermosynechococcus elongatus* BP-1, were amplified from pKM087. The cDNAs of *Fd* and *Fnr* of *Synechocystis* sp. PCC 6803 were synthesized with codon-optimization for humans by GenScript (Piscataway, NJ). The mitochondrial targeting sequence (MTS; MSVLTPLLLRGLTGSARRLP) was derived from human cytochrome C oxidase subunit VIII. These cDNAs were subcloned into the pCAGGS vector (47) to generate pCAGGS-MTS-PcyA, pCAGGS-MTS-PcyA-mCherry, pCAGGS-MTS-HO1-mCFP, pCAGGS-MTS-Fd-mVenus, and pCAGGS-MTS-Fnr-tagBFP. The cDNA of PHFF, which contained MTS-PcyA-FLAG-P2A-MTS-HA-HO1-P2A-MTS-Myc-Fd-P2A-MTS-Fnr-T7, was synthesized by GenScript, and subcloned into the pCAGGS vector to obtain pPHFF. The cDNA sequence of PHFF is included in Fig. S2. pcDNA3.1-UnaG-mCherry was a kind gift from Atsushi Miyawaki (35).

The cDNAs of PhyB (1-908 a.a.), PIF6 (1-100 a.a.), and PIF3 (1-100 a.a.), which were derived from *Arabidopsis thaliana*, were synthesized with codon-optimization for humans by GenScript. According to a previous report (18), the cDNAs of PhyB, linker, mCherry, and the C-terminus of H-Ras (HRasCT), a plasma membrane localization signal, were inserted into the pCAGGS vector to generate pCAGGS-PhyB-mCherry-HrasCT. The Tyr 276 of PhyB was substituted to His by two-step overlap PCR, generating pCAGGS-PhyB-Y276H-mCherry-HRasCT. The cDNA of PhyB (1-621 a.a.) was amplified by PCR to obtain pCAGGS-PhyB621-mCherry-HRasCT. The cDNAs of PIF3 or PIF6 and mEGFP were inserted into the pCAGGS vector to construct pCAGGS-PIF3-mEGFP or pCAGGS-PIF6-mEGFP. The cDNAs of PIF3 and full length human CRaf were fused and subcloned into the pCX4puro vector (48) to produce pCX4puro-PIF3-CRaf. The cDNAs of PIF3, human Tiam1 (952-1532 a.a.) and mEGFP were fused and subcloned into the pCX4bsr vector to generate pCX4bsr-Tiam1-PIF3-mEGFP. pPBbsr-EKAREV-NLS, a *piggyBac* transposon donor vector (49), has been described previously (39). The cDNAs of human *HO1*, *Fd* (ferredoxin-1 also known as

adrenodoxin), and *Fnr* were amplified form a cDNA pool obtained from mRNA of HeLa cells, and subcloned into pCAGGS vector, generating pCAGGS-MTS-hHO1-mCFP, pCAGGS-MTS-hFd-mVenus, and pCAGGS-MTS-hFnr-tagBFP. The details of other plasmids are described in SI Materials and Methods.

Cells and reagents

HeLa cells were purchased from the Human Science Research Resources Bank (Sennanshi, Japan) and maintained in DMEM (Wako, Osaka, Japan) supplemented with 10% FBS (Sigma-Aldrich, St. Louis, MO). HEK-293 cells were maintained in MEM (Sigma-Aldrich, St. Louis, MO) supplemented with 10% FBS. HEK-293T cells were obtained from Invitrogen as Lenti-X 293 cells (Carlsbad, CA), and maintained in DMEM supplemented with 10% FBS. Mouse embryonic stem cells (mESCs) and mouse embryonic fibroblasts (MEFs) was a kind gift of Toshihiko Fujimori (National Institute for Basic Biology, Japan). The mESCs were maintained in DMEM supplemented with 10% FBS , 1% GlutaMAX (Thermo Fisher Scientific, Waltham, MA), 1% non-essential amino acids (Thermo Fisher Scientific), 1% sodium pyruvate (Thermo Fisher Scientific), 1% penicillin streptomycin (Nacalai Tesque), 1000 unit/mL ESGRO Leukemia Inhibitory Factor (Merck, Germany), 4×10^{-4} % 2-mercaptoethanol (Nacalai Tesque), 1 μM PD0325901 (Tocris Bioscience, UK), and 3 μM CHIR99021 (Cayman Chemical Company, Ann Arbor, MI). The MEFs were maintained in DMEM supplemented with 10% FBS.

PCB was purchased from Santa Cruz Biotechnology (Dallas, TX), dissolved in DMSO (final concentration: 5 mM), and stored at -30°C. Biliverdin was purchased from Sigma-Aldrich, dissolved in DMSO (final concentration: 25 mM), and stored at -30°C. Bilirubin was purchased from Wako, dissolved in DMSO and diluted in PBS. Anti-mCherry rabbit polyclonal antibody was obtained from Abcam (Cambridge, UK). The IRDye800CW-conjugated anti-mouse immunoglobulin secondary antibodies were purchased from LI-COR (Lincoln, NE). 5-Aminolevulinic acid hydrochloride (5-ALA) and FeSO4·7H2O (iron(ii) sulfate) was purchased from Sigma-Aldrich, and dissolved in H_2O. We treated cells with 250 μM 5-ALA and 40 μM iron(ii) sulfate for 2 days.

Acknowledgements

We thank W. Weber (pKM087), A. Bradley (PiggyBac), F. Zhang (pX459 and lentiCRISPR v2), H. Miyoshi (pCMV-VSV-G-RSV-Rev), and A. Miyawaki (pcDNA3.1-UnaG-mcherry) for the plasmids, T. Fujimori for mESCs and MEFs, and J. Nakayama for WT fission yeasts A. Kawagishi, K. Hirano, N. Nishimoto, K. Onoda, and E. Ebine are also to be thanked for their technical assistance. We thank the members of the Matsuda Laboratory and the Aoki Laboratory for their helpful input. K.A. and M.M. were supported by the Platform for Dynamic Approaches to Living System from the Ministry of Education, Culture, Sports, and Science, Japan, and CREST, JST. K.A. was supported by JSPS KAKENHI Grant Number 16H01425, 16H01447, and 16KT0069, THE HORI SCIENCES AND ARTS FOUNDATION, and The Nakajima Foundation.

Reference

1. Kholodenko B, Yaffe MB, Kolch W (2012) Computational Approaches for Analyzing Information Flow in Biological Networks. *Sci Signal* 5(220):re1-re1.
2. Kholodenko BNB (2006) Cell-signalling dynamics in time and space. *Nat Rev Mol cell Biol* 7(3):165–176.
3. Mendoza MC, Er EE, Blenis J (2011) The Ras-ERK and PI3K-mTOR pathways: Cross-talk and compensation. *Trends Biochem Sci* 36(6):320–328.
4. Lemmon MA, Schlessinger J (2010) Cell signaling by receptor tyrosine kinases. *Cell* 141(7):1117–1134.
5. Oda K, Matsuoka Y, Funahashi A, Kitano H (2005) A comprehensive pathway map of epidermal growth factor receptor signaling. *MolSystBiol* 1:2005.
6. Fujita Y, Komatsu N, Matsuda M, Aoki K (2014) Fluorescence resonance energy transfer based quantitative analysis of feedforward and feedback loops in

epidermal growth factor receptor signaling and the sensitivity to molecular targeting drugs. *FEBS J* 281(14):3177–3192.

7. Prahallad A, et al. (2012) Unresponsiveness of colon cancer to BRAF(V600E) inhibition through feedback activation of EGFR. *Nature* 483(7387):100–3.
8. Friday BB, et al. (2008) BRAF V600E disrupts AZD6244-induced abrogation of negative feedback pathways between extracellular signal-regulated kinase and Raf proteins. *Cancer Res* 68(15):6145–6153.
9. Inoue T, Meyer T (2008) Synthetic activation of endogenous PI3K and Rac identifies an AND-gate switch for cell polarization and migration. *PLoS One* 3(8). doi:10.1371/journal.pone.0003068.
10. Derose R, Miyamoto T, Inoue T (2013) Manipulating signaling at will: Chemically-inducible dimerization (CID) techniques resolve problems in cell biology. *Pflugers Arch Eur J Physiol* 465(3):409–417.
11. Aoki K, et al. (2013) Stochastic ERK activation induced by noise and cell-to-cell propagation regulates cell density-dependent proliferation. *Mol Cell* 52(4):529–540.
12. Kennedy MJ, et al. (2010) Rapid blue-light-mediated induction of protein interactions in living cells. *Nat Methods* 7(12):973–975.
13. Zhang K, Cui B (2015) Optogenetic control of intracellular signaling pathways. *Trends Biotechnol* 33(2):92–100.
14. Tischer D, Weiner OD (2014) Illuminating cell signalling with optogenetic tools. *Nat Rev Mol Cell Biol* 15(8):551–8.
15. Taslimi A, et al. (2016) Optimized second-generation CRY2–CIB dimerizers and photoactivatable Cre recombinase. *Nat Chem Biol* 12(April):1–8.

16. Kiyokawa E, Hara S, Nakamura T, Matsuda M (2006) Fluorescence (F??rster) resonance energy transfer imaging of oncogene activity in living cells. *Cancer Sci* 97(1):8–15.

17. Endo M, Ozawa T (2017) Strategies for development of optogenetic systems and their applications. *J Photochem Photobiol C Photochem Rev* 30:10–23.

18. Levskaya A, Weiner OD, Lim W a, Voigt C a (2009) Spatiotemporal control of cell signalling using a light-switchable protein interaction. *Nature* 461(7266):997–1001.

19. Shimizu-Sato S, Huq E, Tepperman JM, Quail PH (2002) A light-switchable gene promoter system. *Nat Biotechnol* 20(October):1041–1044.

20. Liou JC, et al. (2001) The new NASA orbital debris engineering model ORDEM2000. *Eur Sp Agency, (Special Publ ESA SP* 1(473):309–313.

21. Toettcher JE, Weiner OD, Lim WA (2013) Using optogenetics to interrogate the dynamic control of signal transmission by the Ras/Erk module. *Cell* 155(6):1422–1434.

22. Gambetta GA, Lagarias JC (2001) Genetic engineering of phytochrome biosynthesis in bacteria. *Proc Natl Acad Sci U S A* 98(19):10566–71.

23. Mukougawa K, Kanamoto H, Kobayashi T, Yokota A, Kohchi T (2006) Metabolic engineering to produce phytochromes with phytochromobilin, phycocyanobilin, or phycoerythrobilin chromophore in Escherichia coli. *FEBS Lett* 580(5):1333–1338.

24. M??ller K, et al. (2013) A red/far-red light-responsive bi-stable toggle switch to control gene expression in mammalian cells. *Nucleic Acids Res* 41(7). doi:10.1093/nar/gkt002.

25. Muramoto T (1999) The Arabidopsis Photomorphogenic Mutant hy1 Is Deficient in Phytochrome Chromophore Biosynthesis as a Result of a Mutation in a Plastid Heme Oxygenase. *Plant Cell Online* 11(3):335–348.

26. Kohchi T (2001) The Arabidopsis HY2 Gene Encodes Phytochromobilin Synthase, a Ferredoxin-Dependent Biliverdin Reductase. *Plant Cell Online* 13(2):425–436.

27. Frankenberg N (2001) Functional Genomic Analysis of the HY2 Family of Ferredoxin-Dependent Bilin Reductases from Oxygenic Photosynthetic Organisms. *Plant Cell Online* 13(4):965–978.

28. Ponka P (1999) Cell Biology of Heme. *Am J Pathol* 318(4):241–56.

29. Ajioka RS, Phillips JD, Kushner JP (2006) Biosynthesis of heme in mammals. *Biochim Biophys Acta - Mol Cell Res* 1763(7):723–736.

30. Fischer AJ, et al. (2005) Multiple roles of a conserved GAF domain tyrosine residue in cyanobacterial and plant phytochromes. *Biochemistry* 44(46):15203–15215.

31. Müller K, et al. (2013) Synthesis of phycocyanobilin in mammalian cells. *Chem Commun* 49(79):8970.

32. Khanna R, et al. (2004) A novel molecular recognition motif Nnecessary for targeting photoactivated phytochrome signaling to specific Basic Helix-Loop-Helix transcription factors. *Plant Cell* 16(11):3033–3044.

33. Anders K, Essen LO (2015) The family of phytochrome-like photoreceptors: Diverse, complex and multi-colored, but very useful. *Curr Opin Struct Biol* 35:7–16.

34. Terry MJ, Maines MD, Lagarias JC (1993) Inactivation of phytochrome- and

phycobiliprotein-chromophore precursors by rat liver biliverdin reductase. *J Biol Chem* 268(35):26099–26106.

35. Kumagai A, et al. (2013) A bilirubin-inducible fluorescent protein from eel muscle. *Cell* 153(7):1602–1611.
36. Rodriguez EA, et al. (2016) A far-red fluorescent protein evolved from a cyanobacterial phycobiliprotein. *Nat Methods* 13(9):763–769.
37. Kamai T, et al. (2003) Significant association of Rho/ROCK pathway with invasion and metastasis of bladder cancer. *Clin Cancer Res* 9(7):2632–2641.
38. Michiels F, et al. (1997) Regulated membrane localization of Tiam1, mediated by the NH2-terminal pleckstrin homology domain, is required for Rac-dependent membrane ruffling and c-Jun NH2-terminal kinase activation. *J Cell Biol* 137(2):387–398.
39. Komatsu N, et al. (2011) Development of an optimized backbone of FRET biosensors for kinases and GTPases. *Mol Biol Cell* 22(23):4647–56.
40. Grinberg A V., et al. (2000) Adrenodoxin: Structure, stability, and electron transfer properties. *Proteins Struct Funct Bioinforma* 40(4):590–612.
41. Ziegler G a, Vonrhein C, Hanukoglu I, Schulz GE (1999) The structure of adrenodoxin reductase of mitochondrial P450 systems: electron transfer for steroid biosynthesis. *J Mol Biol* 289(4):981–990.
42. HANUKOGLU I, GUTFINGER T (1989) cDNA sequence of adrenodoxin reductase: Identification of NADP-binding sites in oxidoreductases. *Eur J Biochem* 180(2):479–484.
43. Baranano DE, Rao M, Ferris CD, Snyder SH (2002) Biliverdin reductase: a major physiologic cytoprotectant. *Proc Natl Acad Sci U S A* 99(25):16093–

16098.

44. Lerner-Marmarosh N, Miralem T, Gibbs PEM, Maines MD (2008) Human biliverdin reductase is an ERK activator; hBVR is an ERK nuclear transporter and is required for MAPK signaling. *Proc Natl Acad Sci U S A* 105(19):6870–5.

45. Maghzal GJ, Leck MC, Collinson E, Li C, Stocker R (2009) Limited role for the bilirubin-biliverdin redox amplification cycle in the cellular antioxidant protection by biliverdin reductase. *J Biol Chem* 284(43):29251–29259.

46. Hinds TD, et al. (2016) Biliverdin reductase A attenuates hepatic steatosis by inhibition of Glycogen Synthase Kinase (GSK) 3β phosphorylation of serine 73 of Peroxisome Proliferator-activated Receptor (PPAR) α. *J Biol Chem* 291(48):25179–25191.

47. Hitoshi N, Ken-ichi Y, Jun-ichi M (1991) Efficient selection for high-expression transfectants with a novel eukaryotic vector. *Gene* 108(2):193–199.

48. Aoki K, Yamada M, Kunida K, Yasuda S, Matsuda M (2011) Processive phosphorylation of ERK MAP kinase in mammalian cells. *Proc Natl Acad Sci U S A* 108(31):12675–12680.

49. Yusa K, Rad R, Takeda J, Bradley A (2009) Generation of transgene-free induced pluripotent mouse stem cells by the piggyBac transposon. *Nat Methods* 6(5):363–369.

Author contributions

Y.U., M.M., and K.A. designed research;Y.U., Y.G., S.O., and K.A. performed experiments; Y.U., Y.G., S.O., and K.A. analyzed the data. Y.U., M.M., and K.A. wrote the paper.

Competing financial interest

The authors declare no conflict of interest.

Figure

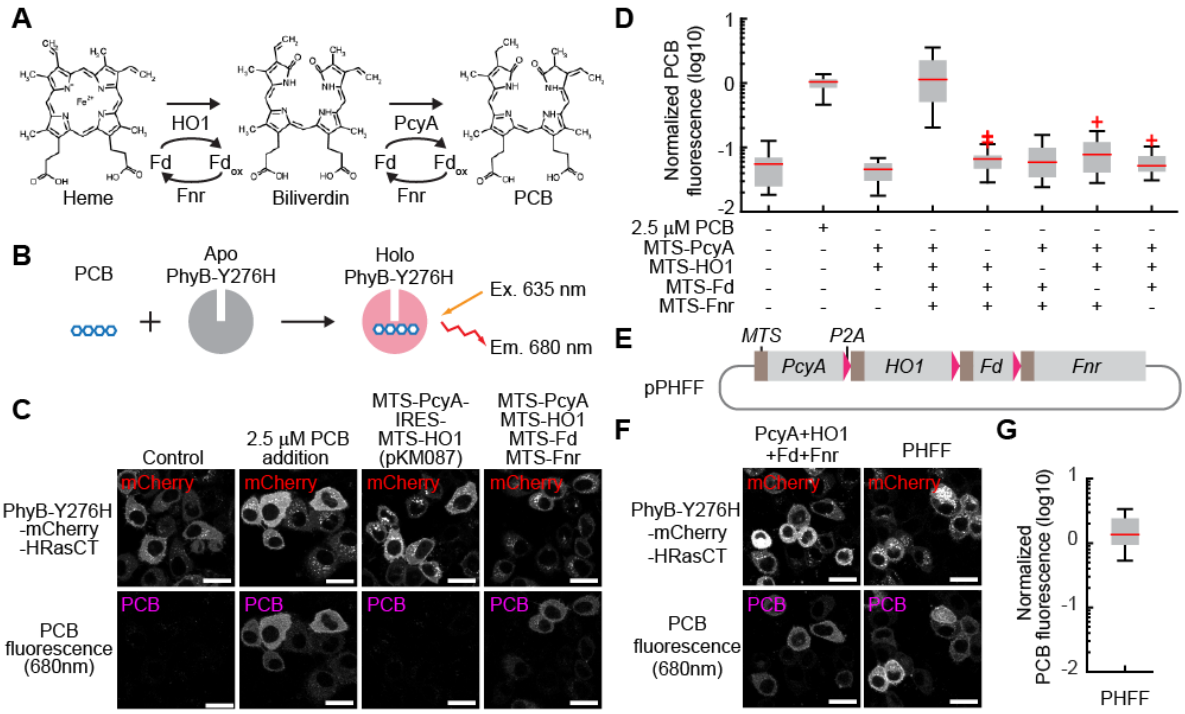

Figure 1 PCB synthesis in mammalian cells

(A) The pathway of PCB synthesis in cyanobacteria. (B) Scheme for measurement of PCB fluorescence. The PhyB mutant, PhyB-Y276H, emits fluorescence from PCB when it binds to PCB. (C) Fluorescence images of PhyB-Y276H-mCherry-HRas C-terminus (HRasCT) (upper) and PCB fluorescence bound to PhyB-Y276H (lower) are shown for the indicated condition in HeLa cells. pKM087 is a bicistronic vector expressing MTS-PcyA and MTS-HO1 (31). Scale bars, 25 μm. (D) Quantification of PCB synthesis. PCB fluorescence bound to PhyB-Y276H was divided by mCherry fluorescence, followed by normalization to the average PCB-bound PhyB-Y276H/mCherry value of 2.5 μM PCB-treated cells. The box extends from the first to the third quartile with the whiskers denoting 1.5 times the interquartile range. Red crosses are outliers. N = 24. (E) Structure of the pPHFF plasmid expressing MTS-PcyA, MTS-HO1, MTS-Fd and MTS-Fnr. These cDNAs are connected by the cDNAs of a self-cleaving 2A peptide, P2A, which allows stoichiometric expression of multiple proteins flanking the 2A peptide. (F) Fluorescence images of PhyB-Y276H-mCherry-HRasCT (upper) and PCB (lower) are shown as in panel D. Scale bars, 20 μm. (G) PCB fluorescence in HeLa cells expressing PHFF was quantified as in panel D. N = 23.

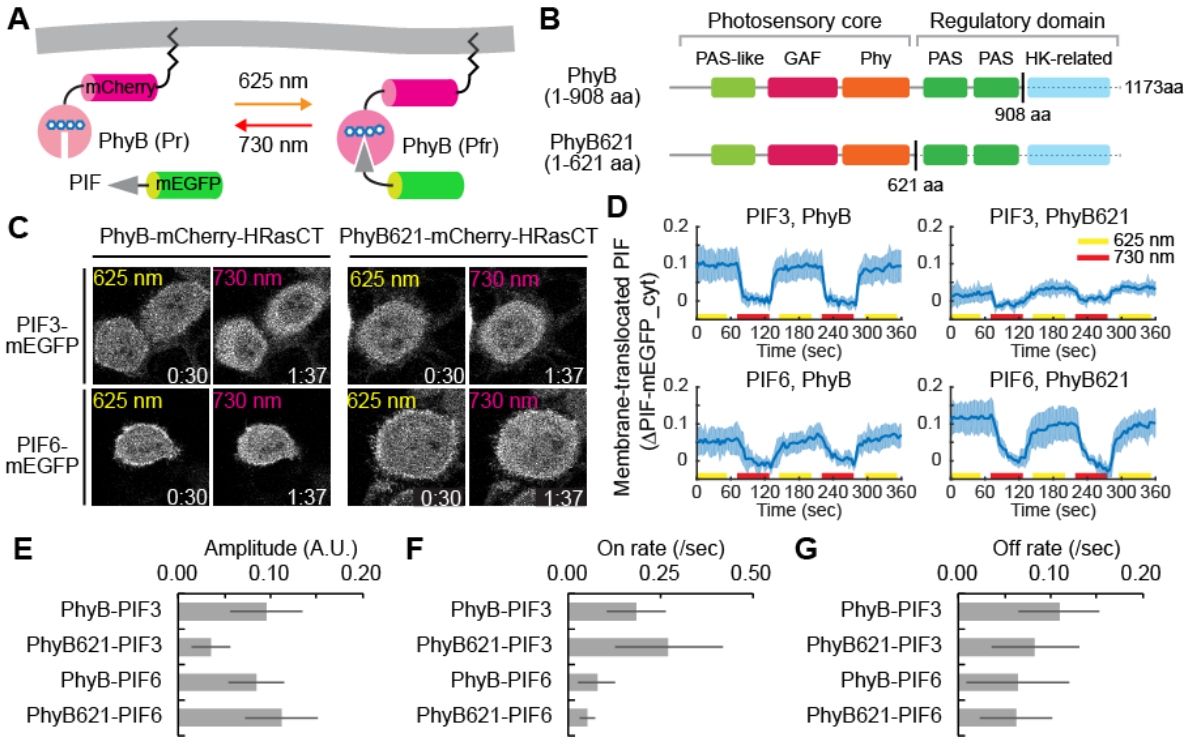

Figure 2 PhyB-PIF LID with endogenously-synthesized PCB

(A) A schematic representation of the PhyB-PIF LID system. PhyB-mCherry-HRasCT is localized at the plasma membrane. PIF fused with mEGFP is translocated to the plasma membrane through the binding to PhyB-mCherry-HRasCT upon illumination with red light (625 nm). Illumination with far-red light (730 nm) induces dissociation of the PhyB-PIF heterodimer. (B) Domain structures of PhyB (1-908 a.a.) and PhyB621 (1-621 a.a.). (C) PhyB-PIF LID assay. PIF-mEGFP fluorescence images are shown in HeLa cells expressing PHFF, PhyB-mCherry-HRasCT (left column) or PhyB621-mCherry-HRasCT (right column), and PIF3-mEGFP (upper row) or PIF6-mEGFP (lower row) upon the illumination with red light (left) and far-red light (right). (D) Membrane-recruited PIF-mEGFP was quantified by the fractional change in the fluorescence intensity of PIF-mEGFP at the cytoplasm in comparison to that under the condition of far-red light exposure. The average values (bold lines) are plotted as a function of time with the SD. N =8. (E-G) Quantification of PhyB-PIF LID. Amplitude (E), On rate (F), and Off rate (G) of PIF membrane translocation were quantified by curve fitting the data in panel D with a single exponential curve. The bar graphs show the average values with the SD. A.U., arbitrary units.

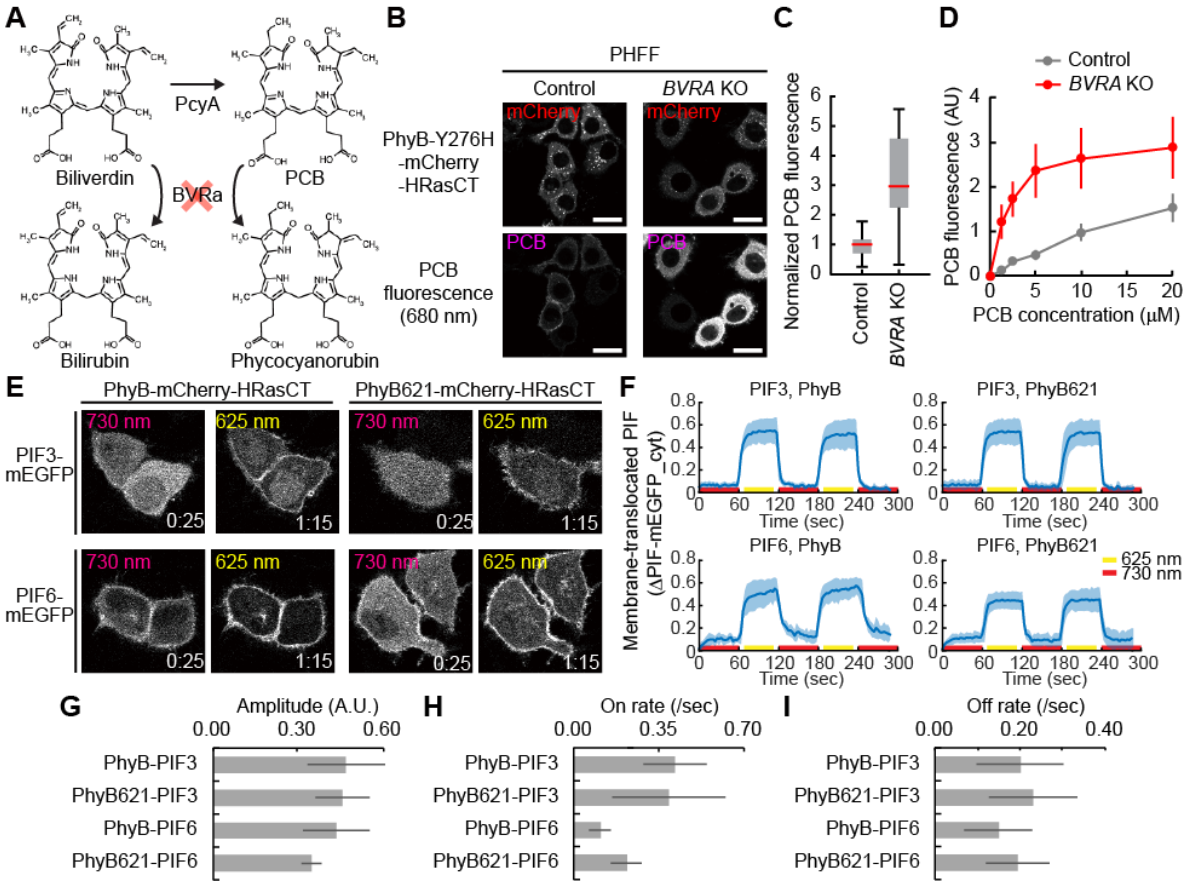

Figure 3 Enhancement of PCB synthesis by knock-out of the biliverdin reductase A gene.

(A) Scheme of the metabolic pathway of biliverdin and PCB. Biliverdin reductase A (BVRA) degrades both biliverdin and PCB, generating bilirubin and phycocyanorubin, respectively. (B) PCB synthesis in control (left) and *BVRA* KO HeLa cells (right). Representative images of PhyBY276H-mCherry-HRas CT (upper) and PCB (lower) are shown as in Fig. 1C. Scale bars, 25 μm. (C) PCB fluorescence in the control and BVRA KO cells was divided by mCherry fluorescence, and normalized to the average PCB/mCherry value in control cells as 1.0. The normalized PCB fluorescence is shown as a box plot as in Fig. 1D. (D) Purified PCB was supplied to control (grey) and *BVRA* KO (red) HeLa cells expressing PhyBY276H-mCherry-HRasCT. PCB fluorescence is plotted as a function of PCB concentration. (E) PhyB-PIF LID assay. PIF-mEGFP fluorescence images are shown in *BVRA* KO HeLa cells as in Fig. 2C. (F) Quantification of PhyB-PIF LID. Membrane-recruited PIF-mEGFP was quantified, and the average values (bold lines) are plotted as in Fig. 2D. N = 8. (G-I) Quantification of

PhyB-PIF LID. Amplitude (G), on rate (H), and off rate (I) of PIF membrane translocation were quantified by curve fitting the data in panel F with a single exponential curve. The bar graphs show the average values with the SD. A.U., arbitrary units.

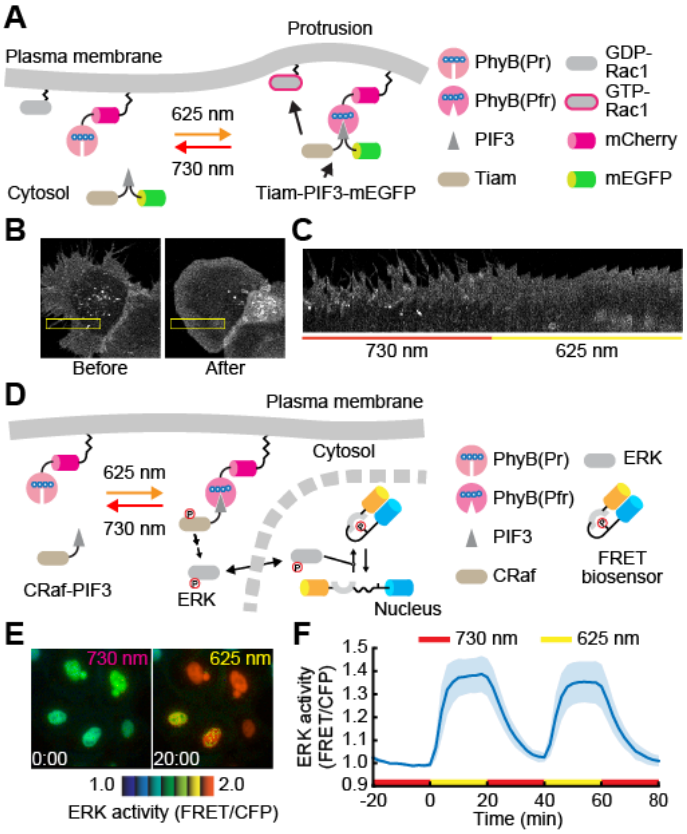

Figure 4 Manipulation of intracellular signaling by the PhyB-PIF system with endogenously-synthesized PCB

(A) Schematic representation of Rac1 activation by the PhyB-PIF system. Tiam1-PIF3-mEGFP, a Rac1 activator, is translocated to the plasma membrane upon exposure to red light, leading to the Rac1 activation. (B and C) *BVRA* KD HEK-293 cells stably expressing PhyB-mCherry-HRasCT, and Tiam1-PIF3-mEGFP were transfected with pPHFF. Two days after trasfectin, the cells were subjected to a far-red light condition (before), followed by a red light condition (after). Fluorescence images of PhyB-mCherry-HRasCT (B), and the montage image in the yellow box of panel B are shown (C). (D) Schematic representation of ERK activation by the PhyB-PIF system.

Recruitment of CRaf-PIF3 to the membrane by PhyB-PIF LID results in ERK activation, which is monitored by a FRET biosensor, EKAREV-NLS. (E and F) *BVRA* KO HeLa cells expressing PHFF, PhyB-mCherry-HRasCT, CRaf-PIF3, and EKAREV-NLS were imaged under the conditions of far-red light and red light illumination. Images of ERK activity are represented in the IMD mode (E). The average ERK activity (normalized FRET/CFP ratio) was quantified and plotted as a function of time with the SD (F). N = 9.

Table S1. Fission yeast strain list

Strain	Genotype	Origin	Figure
YG051	h- c1::Padh1-MTS-PcyA-FLAG<<kan	972 tf	
YG073	h- c1::Padh1-PHFF<<kan	972 tf	
YG075	h- c1::Padh1-MTS-PcyA-FLAG<<kan c2::Padh1-MTS-HA-HO1<<bsd	YG051 tf	
YG103	h- ade6-M216 leu1-32 z1::Padh1-PhyB621-Y276H-mCherry<<hyg	TN366 tf	Fig. S3A, B
YG084	h+ ade6-M216 leu1-32 z1::Padh1-PhyB621-Y276H-mCherry<<bsd	TN366 tf	Fig. S3A, B
YG090	h- leu1? z1::Padh1-PhyB621-Y276H-mCherry<<bsd c1::Padh1-PHFF<<kan	YG73xYG84	Fig. S3C, D
YG102	h- z1::Padh1-PhyB621-Y276H-mCherry<<hyg	972 tf	Fig. S3C, D
YG107	h? leu? c1::Padh1-MTS-PcyA-FLAG<<kan c2::Padh1-MTS-HA-HO1<<bsd z1::Padh1-PhyB621-Y276H-mCherry<<hyg	YG75xYG103	Fig. S3C, D
YG090	h- leu1? z1::Padh1-PhyB621-Y276H-mCherry<<bsd c1::Padh1-PHFF<<kan	YG73xYG84	

SI Materials and Methods

Plasmids

pSpCas9(BB)-2A-Puro (pX459) and lentiCRISPR v2 were gifts from Feng Zhang (Addgene plasmids # 62988 and #52961, respectively) (5). pX459-BVRA was generated by annealing the sgRNA oligo inserts, followed by subcloning into the pX459 vector. The sgRNA targets the following sequence of the human *BVRA* gene: 5'-CCGCAAGTCCCTCATCCGCACGG-3'. The PAM sequence is underlined. As a control, lentiCRISPRv2-RLuc, which targeted *Renilla Luciferase*, was generated according to the above-described protocol. The sgRNA targets the following sequence of the *Renilla Luciferase* gene: 5'- AGGTGTACGACCCCGAGCAGAGG-3'. The shRNA-targeting human BVRA construct, pSUPER-sh-hBVRA (#1) and pSUPER-sh-hBVRA (#2), was generated by using pSUPER.retro.puro vector (OligoEngine, Seattle, WA). The 22-nucleotide sequences used to target the human *BVRA* gene were 5'-CATATACTGATCTTCCTTTCGC-3' (#1) and 5'-GATCTTTCAGAAATATGTTCTT-3' (#2). To generate pPHFF-sh-hBVRA (#1) and pPHFF-sh-hBVRA (#2), H1 promoter and sh-hBVRA sequence were amplified by PCR, and subcloned into pPHFF by Gibson assembly (6). pPHFF-sh-mBVRA, which expressed PHFF and shRNA targeting to mouse BVRA, was generated as in pPHFF-sh-hBVRA. The 21-nucleotide sequences used to target the mouse *BVRA* gene were 5'-GCCAAATGTAGGAGTCAATAA-3'.

Establishment of stable cell lines

HeLa cells were transfected with lentiCRISPRv2-RLuc or pX459-BVRA by 293fectin (Invitrogen, Carlsbad, CA). Two days after transfection, the cells were selected by treatment with 1.0 μg/mL puromycin for 48 h, followed by single cell cloning to establish control HeLa cells or *BVRA* KO HeLa cells. HeLa cells stably expressing EKAREV-NLS were generated as previously reported (4).

For retroviral production, HEK-293T cells were co-transfected with each pCX4 vector or pSUPER vector (7), pGP, and pCMV-VSV-G-RSV-Rev, a gift from Dr. Miyoshi (RIKEN BioResource Center, Ibaraki, Japan), by using polyethyleneimine "Max" MW 40,000 (Polyscience Inc., Warrington, PA). For lentiviral production, HEK-

293T cells were were co-transfected with pCSIIbleo or pCSIIbleo-PHFF vector, psPAX2, a gift from Didier Trono (Addgene plasmid # 12260), and pCMV-VSV-G-RSV-Rev. Virus-containing media were collected at 48 h after transfection, filtered, and applied to target cells with 10 μg/ml polybrene (Nacalai Tesque, Kyoto, Japan). Two days after infection, the infected cells were selected with the following antibiotics: 10 μg/mL blasticidin S (InvivoGen, San Diego, CA), 200 μg/mL hygromycin (Wako), 800 μg/mL G418 (InvivoGen, San Diego, CA), and 1.0 μg/mL puromycin (InvivoGen). The infected mESCs were selected with the following antibiotics: 1.0 μg/mL puromycin and 10 μg/mL zeocin (InvivoGen).

***Schizosaccaharomyces pombe* strain construction and cell culture**

All fission yeast strain used in this study are listed in the Table S1 with their genotypes and origins. They are made from WT strains, 972 (h-) or TN366 (h+ ade6-M216 leu1-32) by transformation and crossing. Growth medium, sporulation medium and other techniques for fission yeast were based on the protocol as described previously (8) unless otherwise noted.

To generate PhyB expressing fission yeast cells, construction cassette was inserted at the gene free region of chromosome II (adjacent to the zfs1+ gene locus: Z1, see primer lists described below). The construction cassette contains genes of PhyB-Y276H fused with mCherry and expressed under the constitutively active adh1 promoter. The terminator sequence of adh1 was set downstream of PhyB stop codon. The selection marker (kan^R, hyg^R, nat^R or bsd^R) was placed in the end of cassette. The construction cassettes were created by the sewing PCR by KOD FX Neo (TOYOBO, KFX-201). PCR product were EtOH precipitated and transformed into cells according to the high-efficiency transformation method (9). Transformed cells were placed on the non-selective YEA plate and incubated at 32℃ for 20 hours, followed by the replica to selection YEA plates containing drugs (100 μg/ml G418 (Invitrogen, 23986-84), 50 μg/ml Hygromicene B (Wako, 085-06153), 100 μg/ml ClonNAT (GOLDBIO.com, N-500-1), 10 μg/ml Blasticidin S (Invitrogen, 03759-71)). PHFF gene and PcyA and HO1 genes were also introduced by the same method as PhyB. They were inserted at the gene free region adjacent to the zfs1+ (Z1; chromosome II) or hgh1+(C1, C2;

chromosome I) gene loci. See also primer lists described below. The genes of PhyB-Y276H, PcyA, and HO1 are human-codon optimized. In order to make the strains having more than one insertions were made by crossing. Different mating type strains were mixed and suspended into Leucine solution and spot on the SPA plate. One day after incubation at 25℃, spore formation was checked by microscope and random spore was done. Asci were incubated with 2% glusurase (PerkinElmer, NEE154001EA) for 2 hour at room temperature, and then spread onto selection plates.

The following primers were used for generating fission yeast strains in this study: C1F1, AGAGATTCGCGAAGTTTG; C1 F2 connect to Padh, TGTTGTAGGGCATGCtgtctgcataacccattt; C1 R2 connect from Ttef, ACGCCGCCATCCAGTgcagagcacaccaaagaa; C1 R1, tggattaatgatatgatg; C2 F1, tgtgttaactcacttaag; C2 F2 connect to Padh, TGTTGTAGGGCATGCactgagcgacgaaccaag; C2 R2 connect from Ttef, ACGCCGCCATCCAGTccttgctctgatcgtttg; C2 R1, agcgatactacactgtgg; Z1 F1, acactacagtgttgaaatg; Z1 F2 connect to Padh, TGTTGTAGGGCATGCtgaatggaagaacaatta; Z1 R2 connect from Ttef, ACGCCGCCATCCAGTttggagagtattggcgat; Z1 R1, ccaaaattcaatcatcac.

Fluorescence imaging with confocal microscope.

HeLa cells and HEK-293 cells were plated on poly-L-lysine (PLL)-coated 35-mm glass-base dishes coated with collagen type I. The plasmids expressing PhyB:PIF-mEGFP:PHFF were transfected by 293fectin at a ratio of 50:1:50. After 48 h, the medium was replaced with FluoroBrite D-MEM (Thermo Fisher Scientific) supplemented 1% GlutaMAX (Thermo Fisher Scientific) and 0.1% bovine serum albumin (BSA). mESC cells were plated on poly-L-lysine (PLL)-coated 35-mm glass-base dishes coated with 0.1 % Gelatin. MEF cells were plated on poly-L-lysine (PLL)-coated 35-mm glass-base dishes. The plasmids expressing PhyB:PIF-mEGFP:PHFF were transfected by Lipofectamine 3000 (Thermo Fisher Scientific) at a ratio of 10:1:10. After 72 h, the medium was replaced with FluoroBrite D-MEM supplemented 1% GlutaMAX and 0.1% bovine serum albumin (BSA). The fission yeast cells were cultured with liquid YEA media at 32℃ to $5.0*10^6$ cells/mL. The cells were washed

and suspended with liquid MM media. For the addition of exogenous PCB to fission yeast, PCB solution was added to $1.0*10^6$ cells/mL cell culture, followed by 6 hours shake at 32℃ for PCB to permeate into the cells. Cell suspension was mounted on the slide glass (Matsunami, MAS-01) and covered by cover glass (Matsunami, 18x18mm No.1).

For confocal fluorescence imaging, cells were imaged with an IX81 inverted microscope (Olympus, Tokyo, Japan) equipped with an FV1000 confocal imaging system (Olympus) or a TCS SP5 microscope (Leica Microsystems, Germany). In Olympus FV1000 confocal imaging system, an oil immersion objective lens (UPLANSAPO 60X O/NA1.35; Olympus) was used. The excitation laser and fluorescence filter settings were as follows: excitation laser, 488 nm (mEGFP), 559 nm (mCherry) and 635 nm (PCB fluorescence); excitation dichroic mirror, DM 405/488/559 dichroic mirror; 500-545 nm (mEGFP), 570-625 nm (mCherry), and 655-755 nm (PCB fluorescence). LEDs for the illumination with red (625 nm) and far-red (735 nm) light were purchased from Optocode (Tokyo, Japan), and controlled manually. In Leica TSC SP5 confocal imaging system, an oil immersion objective lens (HCX PL APO 63 / x1.4–0.6 oil ; Leica Microsystems) was used. The excitation laser and fluorescence filter settings were as follows: excitation laser, 488 nm (mEGFP) and 633 nm (PCB fluorescence); excitation dichroic mirror, TD 488/543/633 dichroic mirror; detector, HyD 520-590 nm (mEGFP) and HyD 670-720 nm (PCB fluorescence). LEDs for the illumination with red (625 nm) and far-red (735 nm) light were purchased from Optocode (Tokyo, Japan), and controlled manually. For

Fluorescence imaging with epi-fluorescence microscope.

HeLa cells expressing EKAREV-NLS were plated on PLL-coated 35-mm glass-base dishes, and transfected with plasmids (PhyB:PIF:PHFF=1:1:1) by 293fectin. Two days after transfection, the cells were starved for 3 h with FluoroBrite D-MEM supplemented 1% GlutaMAX and 0.1% BSA. Imaging was performed with an inverted microscope IX81 (Olympus) equipped with an oil immersion objective lens (UPlanSApo 60x/1.35; Olympus), a Retiga 4000R cooled CCD camera (Photometrics, Tucson, AZ), a Spectra-X light engine (Lumencor Inc., Beaverton, OR), an IX2-ZDC laser-based autofocusing

system (Olympus), a MAC5000 controller for filter wheels and XY stage (Ludl Electronic Products, Hawthorne, NY), and an incubation chamber (Tokai Hit, Shizuoka, Japan). The microscope was controlled by MetaMorph software (Molecular Devices, Sunnyvale, CA). LEDs for the illumination with red (625 nm) and far-red (735 nm) light were were purchased from OptoCode (Tokyo, Japan), and controlled manually. The images were analyzed by MetaMorph software. FRET/CFP ratio images are shown in the intensity-modulated display mode, in which eight colors from red to blue are used to represent the FRET/CFP ratio, with the intensity of each color indicating the mean intensity of FRET and CFP.

Control and BVRA KO HeLa cells were plated on PLL-coated 35-mm glass-base dishes, and transfected with plasmids encoding UnaG-mCherry by 293fectin. Three hour after transfection, the medium was replaced with FluoroBrite D-MEM supplemented 1% GlutaMAX and 0.1% BSA. One day after transfection, cells were imaged with the aforementioned epi-fluorescence microscope.

Zinc blotting and immunoblotting

Cells were lysed in 1xSDS sample buffer. After sonication, the samples were separated by 7.5% SDS-polyacrylamide gel electrophoresis (Nagaiki precast gels; Oriental Instruments, Ltd., Japan). The gel was incubated in buffer containing 150 mM zinc acetate and 150 mM Tris-HCl (pH 6.8) for 3 h. PCB fluorescence was detected by using an Odyssey infrared scanner (LICOR) with 680 nm excitation light. For immunoblotting, proteins were separated by SDS-PAGE, and transferred to polyvinylidene difluoride membranes (Millipore, Billerica, MA). After blocking with 2.5% skim milk (Morinaga, Tokyo, Japan) in TBS-T for 1 h, the membranes were incubated with primary antibodies diluted in blocking buffer, followed by secondary antibodies diluted in blocking buffer. Proteins were detected by an Odyssey infrared scanner (LICOR).

Cell growth assay

HeLa cells or mESCs were plated 1.0×10^4 cell per well in each well of 6-well plate. The cell number were counted every day by Coutness (Thermo Fisher Scientific). The

experimental growth curves was fitting with the following equation.

$$N(t) = A_0 \exp(kt)$$

$N(t)$ and k indicates cell number at the time t and growth rate (/day). A_0 is the initial cell number at the time = 0, namely 1.0×10^4.

SI References

1. Levskaya A, Weiner OD, Lim W a, Voigt C a (2009) Spatiotemporal control of cell signalling using a light-switchable protein interaction. *Nature* 461(7266):997–1001.
2. Aoki K, Yamada M, Kunida K, Yasuda S, Matsuda M (2011) Processive phosphorylation of ERK MAP kinase in mammalian cells. *Proc Natl Acad Sci U S A* 108(31):12675–12680.
3. Yusa K, Rad R, Takeda J, Bradley A (2009) Generation of transgene-free induced pluripotent mouse stem cells by the piggyBac transposon. *Nat Methods* 6(5):363–369.
4. Komatsu N, et al. (2011) Development of an optimized backbone of FRET biosensors for kinases and GTPases. *Mol Biol Cell* 22(23):4647–56.
5. Ran F, Hsu P, Wright J, Agarwala V (2013) Genome engineering using the CRISPR-Cas9 system. *Nat Protoc* 8(11):2281–308.
6. Gibson DG, et al. (2009) Enzymatic assembly of DNA molecules up to several hundred kilobases. *Nat Methods* 6(5):343–5.
7. Akagi T, Sasai K, Hanafusa H (2003) Refractory nature of normal human diploid fibroblasts with respect to oncogene-mediated transformation. *Proc Natl Acad Sci U S A* 100(23):13567–72.

8. Moreno S, Klar A, Nurse P (1991) Molecular genetic analysis of fission yeast Schizosaccharomyces pombe. *Methods Enzymol* 194:795–823.

9. Suga M, Hatakeyama T (2005) A rapid and simple procedure for high-efficiency lithium acetate transformation of cryopreserved Schizosaccharomyces pombe cells. *Yeast* 22(10):799–804.

Supplementary Figure

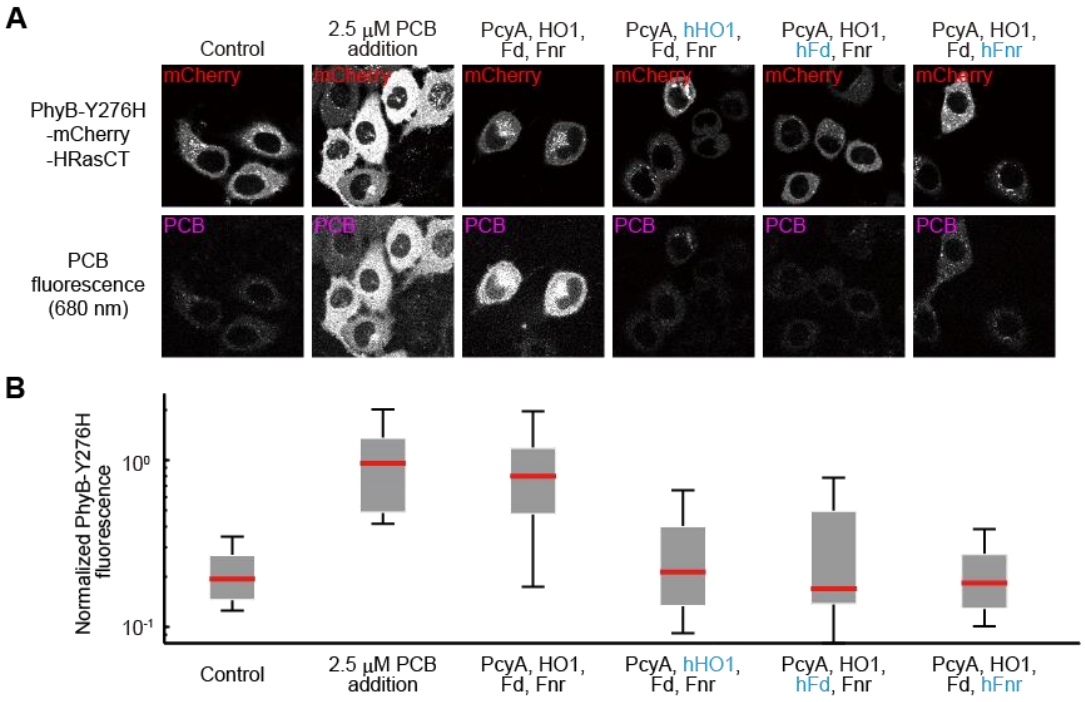

Figure S1: Human HO1, Fd, or Fnr was unable to substitute for HO1, Fd, Fnr in PCB synthesis.

(A) Fluorescence images of PhyB-Y276H-mCherry-HRas C-terminus (HRasCT) (upper) and PCB-bound PhyB-Y276H (lower) are shown for the indicated condition in HeLa cells.. PCB fluorescence was diminished by replacing HO1, Fd, or Fnr with human HO1 (hHO1), human Fd (hFd), or human Fnr (hFnr). (B) Quantification of PCB synthesis. PCB-bound PhyB-Y276H fluorescence was divided by mCherry fluorescence, followed by normalization to the average PCB-bound PhyB-Y276H/mCherry value of 2.5 μM PCB-treated cells. The box extends from the first to the third quartile with the whiskers denoting 1.5 times the interquartile range. Red crosses are outliers. N = 28.

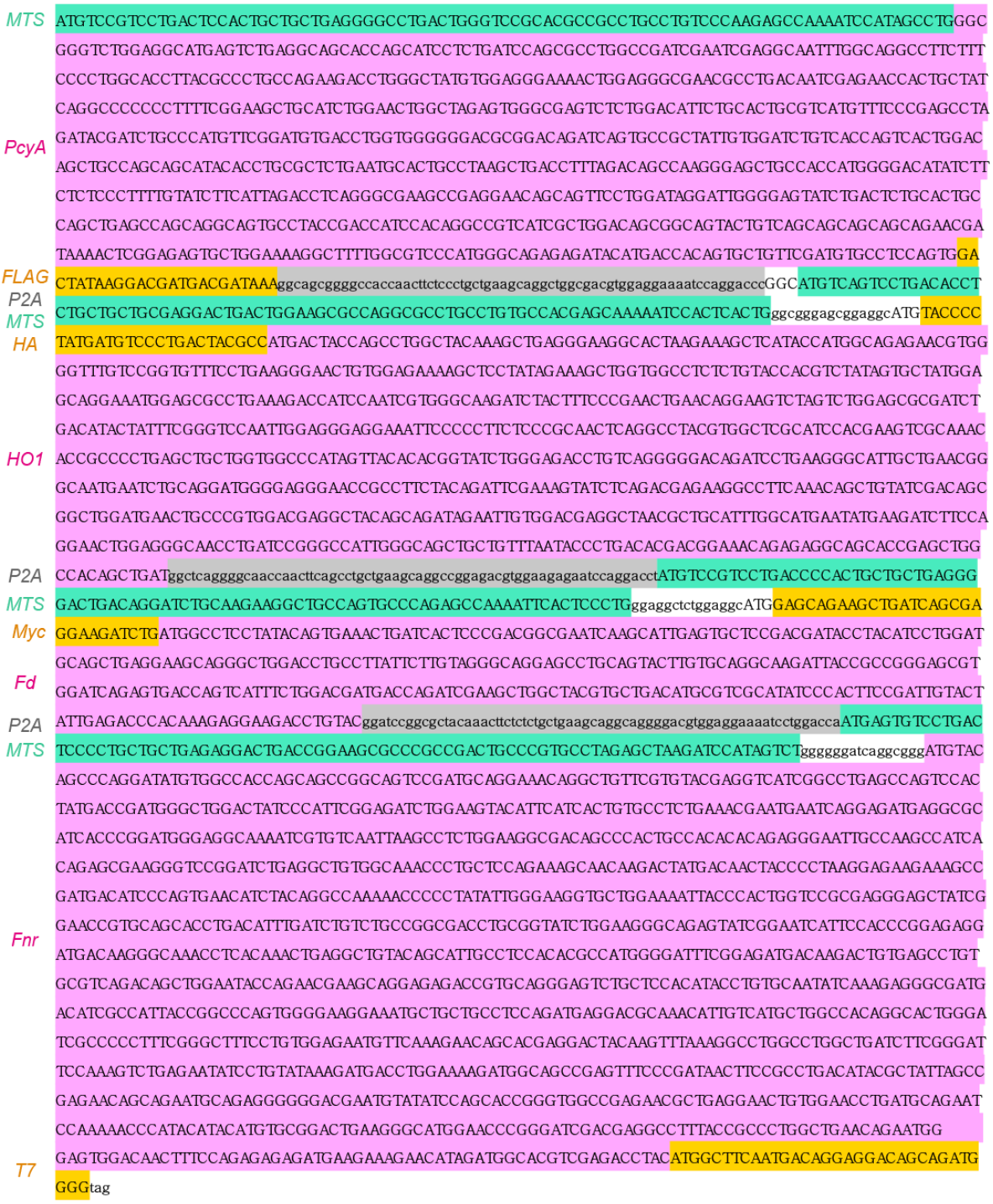

Figure S2: DNA sequence of PHFF.

DNA sequence of PHFF is shown with the indication of individual genes at left.

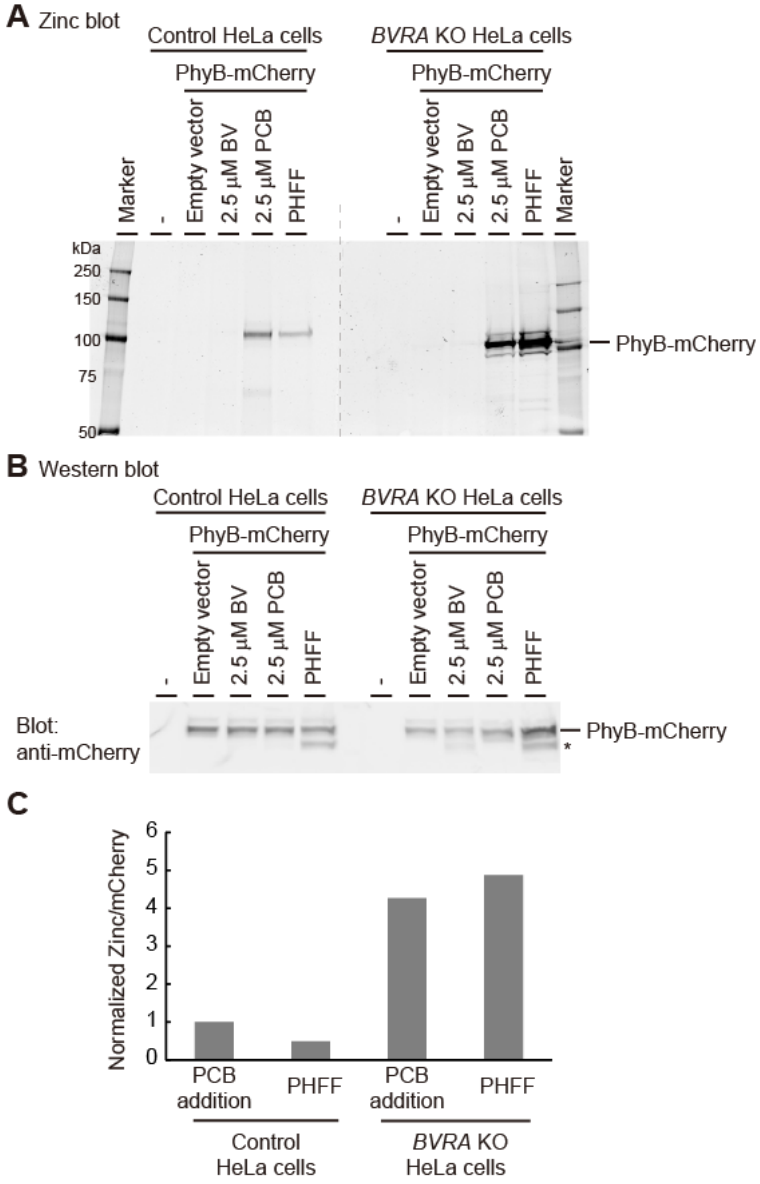

Figure S3: Zinc blot analysis of PCB-bound PhyB.

(A-C) HeLa cells expressing PhyB-mCherry-HRasCT and/or PHFF were treated under the following conditions. BV, 2.5 μM biliverdin for 30 min; PCB, 2.5 μM purified PCB for 30 min. Left half and right half samples were derived from control HeLa and *BVRA* KO HeLa cells, respectively. Cell lysates were separated by SDS-PAGE, followed by detection of PCB fluorescence bound to zinc (A) and mCherry with anti-mCherry antibody (B) by using an Odyssey infra-red imaging system. An asterisk shows the extra bands produced for unknown reasons. Signals of PhyB-mCherry-HRasCT in Zinc blot (A) were devided by those in Westen blotting (B), and then normalized by dividing by the value in control HeLa cells treated with 2.5 μM PCB (C).

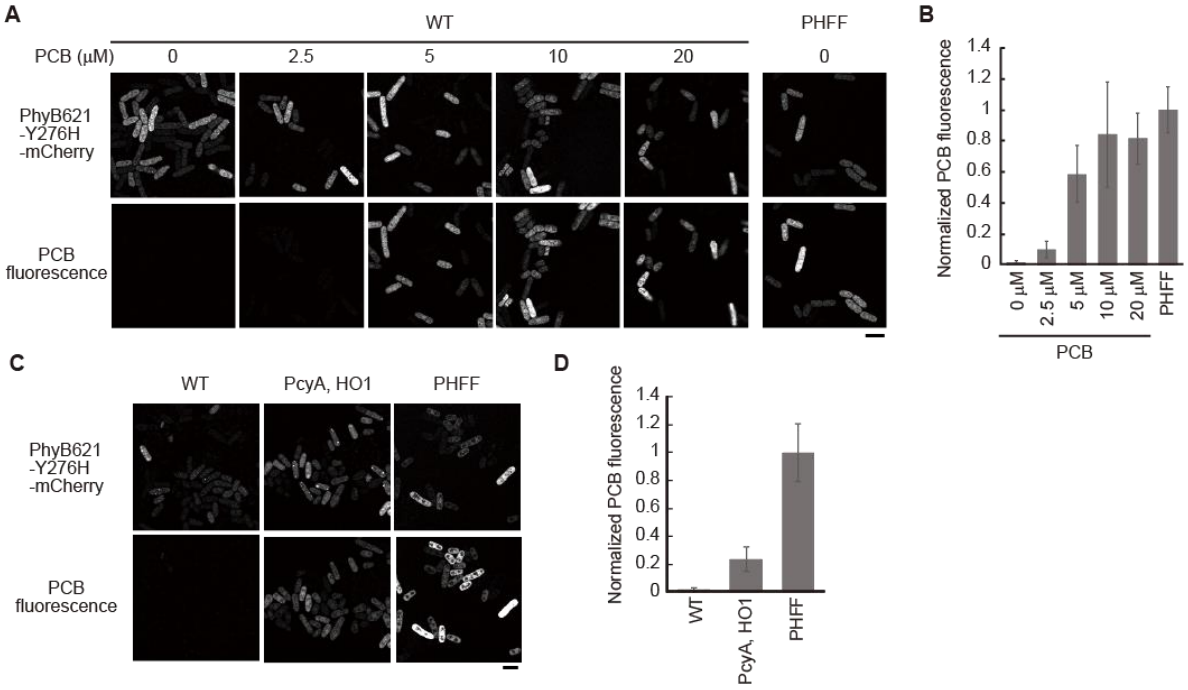

Figure S4: PCB synthesis in fission yeasts.

(A) Representative images of PhyB-Y27H-mCherry fluorescence (upper) and PCB fluorescence (lower) in WT cells treated with the indicated concentration of PCB (left) and PHFF-introduced cell (right). Scale bar, 10 μm. (B) Quantification of PCB synthesis. PCB fluorescence in panel A was divided by mCherry fluorescence, and normalized to the average PCB/mCherry value in PHFF-introduced cells as 1.0. The normalized PCB/mCherry is shown in the bar graph with the SD. N=211 (0 μM), 117 (2.5 μM), 126 (5 μM), 174 (10 μM), 97 (20 μM) and 112 (PHFF) cells. (C) Representative images of PhyB-Y27H-mCherry fluorescence (upper) and PCB fluorescence (lower) in WT cells (left), PcyA and HO1-expressing cells (middle), and PHFF-introduced cells (right). Scale bar, 10 μm. (D) The PCB synthesis was quantified as in panel B. N = 50 for all conditions.

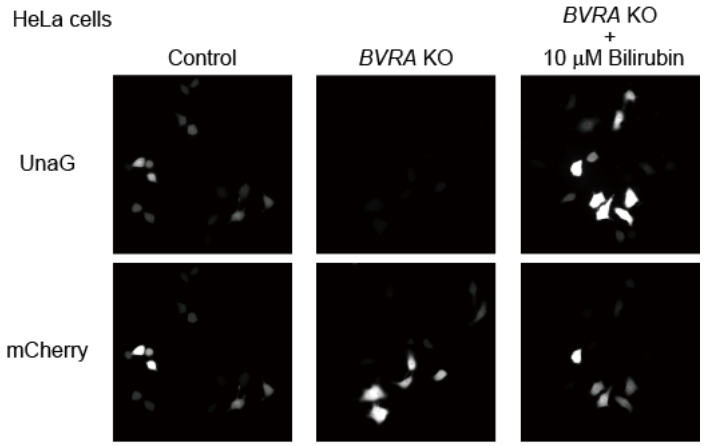

Figure S5: Detection of Bilirubin by UnaG fluorescence in control and BVRA KO HeLa cells.

Control and *BVRA* KO HeLa cells expressing UnaG and mCherry, which was a transfection marker, were treated with or without 10 μM bilirubin for 30 min. The cells were imaged with an epifluorescence microscope. UnaG fluorescence was clearly diminished by *BVRA* KO cells, showing the predominant role of BVRA in bilirubin synthesis.

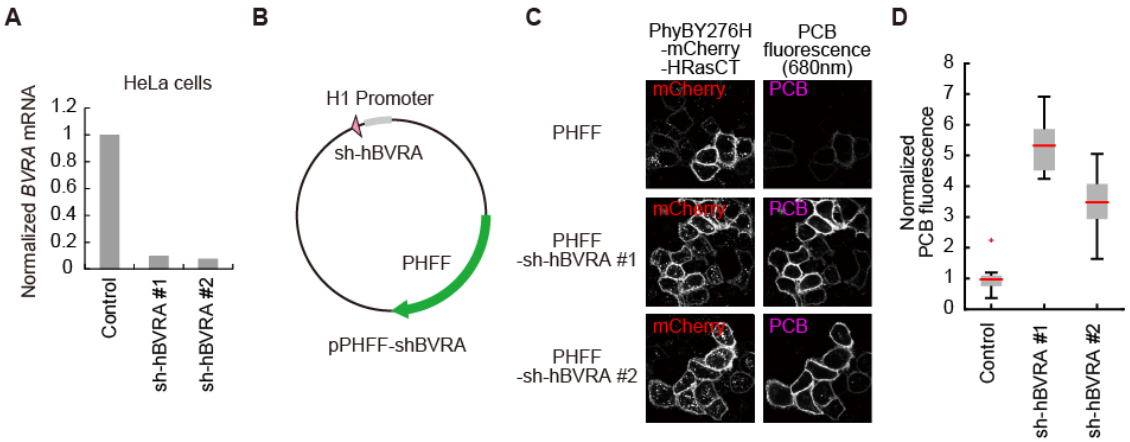

Figure S6: Increase in PCB synthesis by the depletion of BVRA with shRNA.

(A) mRNAs levels of *BVRA* in HeLa cells transfected with control, human *BVRA* shRNA-expressing (#1) and shRNA (#2)-expressing vectors were measured by quantitative PCR. (B) Schematic representation of pPHFF-sh-hBVRA. (C) Fluorescence images of mCherry (left) and PCB (right) in control, BVRA shRNA #1,

and #2 HeLa cells expressing PhyBY276H-mCherry-HrasCT and PHFF. (D) The box plot represents the normalized PCB fluorescence in panel C. N = 12. The box plot was prepared as in Fig. 3C.

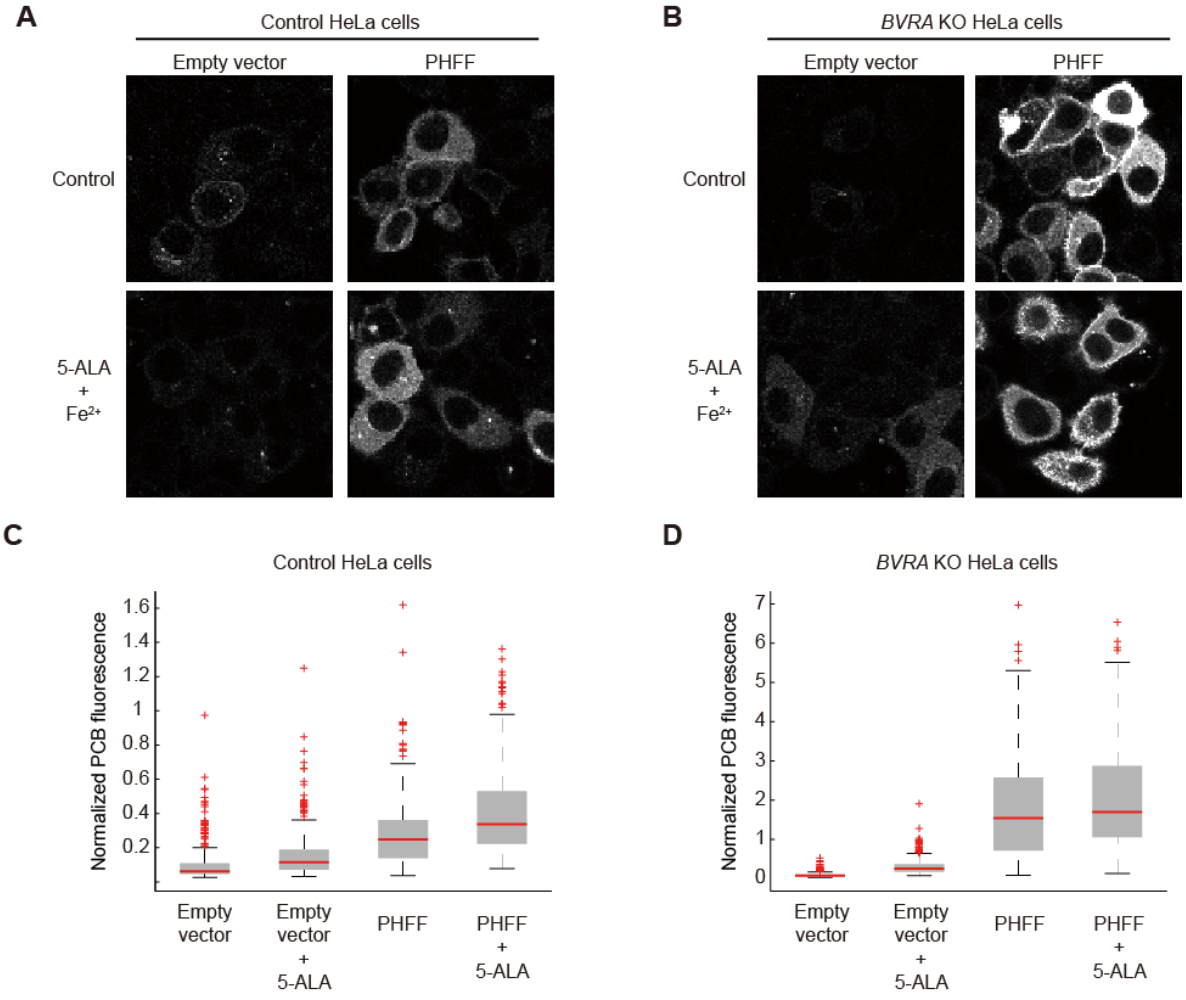

Figure S7: The effect of 5-ALA and iron(ii) sulfate on PCB synthesis.
(A and B) Fluorescence images of PCB-bound PhyB-Y276H are shown for the indicated condition in control HeLa cells (A) and *BVRA KO* HeLa cells (B). (C and D) Quantification of PCB synthesis in control HeLa cells (C) and *BVRA* KO HeLa cells (D). PCB-bound PhyB-Y276H fluorescence was divided by mCherry fluorescence. The box extends from the first to the third quartile with the whiskers denoting 1.5 times the interquartile range. Red crosses are outliers. N > 200 in all experimental conditions.

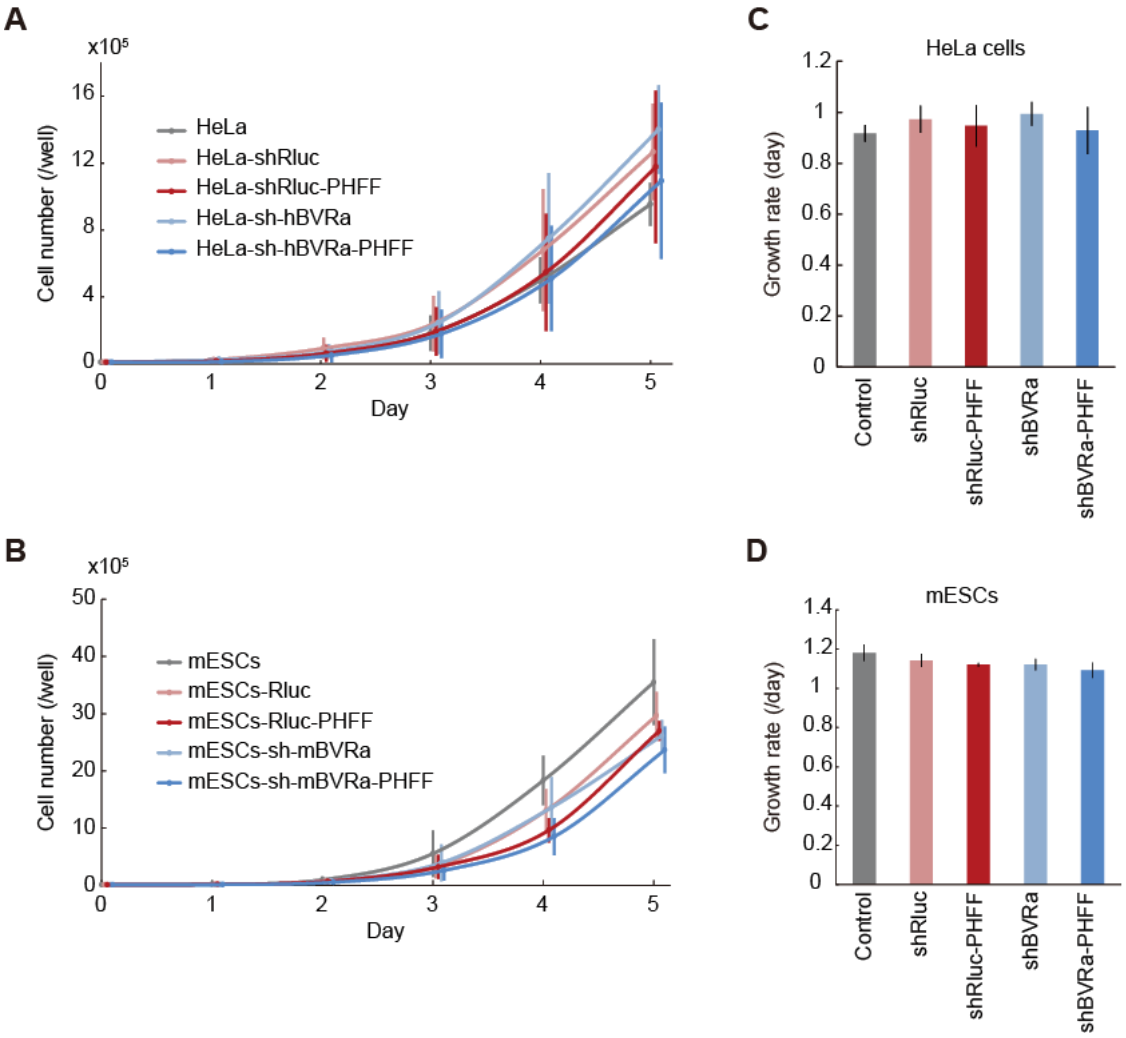

Figure S8: Cell growth rates with or without PCB synthesis in HeLa cells and mESCs.

(A and B) The averages of cell numbers in HeLa cells (A) and mouse embryonic stem cells (mESCs) (B) are plotted as a function of time (day) after seeding with the SD (N = 3). Gray line, parental cells; light red, shRNA against *RLuc* gene (shRuc) for control and Bleomycin resistance gene introduced cells; dark red, shRluc and PHFF introduced cells; light blue, shRNA against BVRA gene (shBVRA) and Bleomycin resistance gene introduced cells; dark blue, shBVRA and PHFF introduced cells. The averages of cell numbers are plotted as a function of time with the SD (N = 3). (C and D) The growth rates in HeLa cells (C) and mESCs (D) were quantified by curve fitting with the data in panels A and B, respectively. The averaged growth rates (/day) are represented in the bar graphs with the SD (N = 3). The *p*-values were 0.61 (C) and 0.07 (D), which were obtained by one-way ANOVA

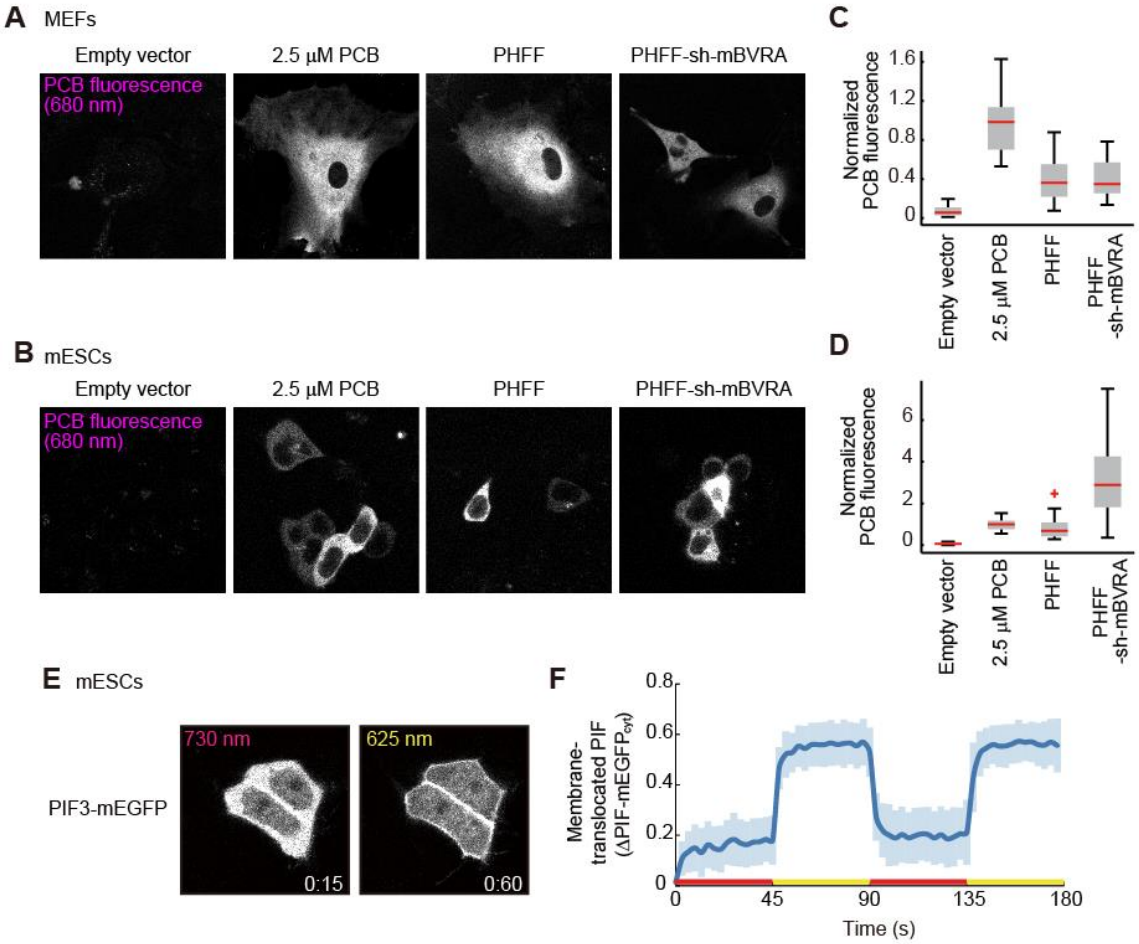

Figure S9: PCB synthesis and PhyB-PIF LID system in mESCs and MEFs.
(A and B) Fluorescence images of PCB-bound PhyB-Y276H are shown for the indicated condition in mouse embryonic fibroblasts (MEFs) (A) and mouse embryonic stem cells (mESCs) (B). PHFF-sh-mBVRA is a co-expression vector for PHFF and shRNA targeting to mouse *BVRA* (mBVRA) as shown in Fig. S6. (C and D) Quantification of PCB synthesis in MEFs (C) and mESCs (D). PCB fluorescence that bound to PhyB-Y276H-mVenus was divided by mVenus fluorescence, followed by normalization to the average PCB-bound PhyB-Y276H/mVenus value of 2.5 μM PCB-treated cells. N = 12 for MEFs. N = 32 for mESCs. (E) PhyB-PIF LID system in mESCs. PIF3-mEGFP fluorescence images are shown in mESCs expressing PhyB-mCherry-HrasCT, PIF3-mEGFP and PHFF-sh-mBVRA. (F) Quantification of PhyB-PIF LID in mESCs. Membrane-recruited PIF-mEGFP was quantified, and the average values (bold lines) are plotted with SD (N = 10) as in Figure 2D.

Moive legends

Movies are available at http://www.pnas.org/content/114/45/11962

Movie S1: Recruitment and dissociation of PIF-mEGFP in HeLa cells expressing PHFF.

HeLa cells expressing following proteins were imaged with red and far-red illumination. (Upper left) PHFF, PhyB-mCherry-HRasCT, PIF3-mEGFP; (upper right) PHFF, PhyB621-mCherry-HRasCT, PIF3-mEGFP; (lower left) PHFF, PhyB-mCherry-HRasCT, PIF6-mEGFP; (lower right) PHFF, PhyB621-mCherry-HRasCT, PIF6-mEGFP. Timestamp shows time in minutes:seconds.

Movie S2: Recruitment and dissociation of PIF-mEGFP in BVRA KO HeLa cells expressing PHFF.

BVRA KO HeLa cells expressing following proteins were imaged with red and far-red illumination. (Upper left) PHFF, PhyB-mCherry-HRasCT, PIF3-mEGFP; (upper right) PHFF, PhyB621-mCherry-HRasCT, PIF3-mEGFP; (lower left) PHFF, PhyB-mCherry-HRasCT, PIF6-mEGFP; (lower right) PHFF, PhyB621-mCherry-HRasCT, PIF6-mEGFP. Timestamp shows time in minutes:seconds.

Movie S3: Regulation of lamellipodial formation by the membrane recruitment of Tiam1 in BVRA KD HEK-293 cells.

BVRA KD HEK-293 cells stably expressing PhyB-mCherry-HRasCT and Tiam1-PIF3-mEGFP were transfected with pPHFF. Two days after transfection, the cells were imaged with confocal microscopy. Timestamp shows time in minutes:seconds.

Movie S4: Repeated ERK activation by membrane recruitment of CRaf in BVRA KO HeLa 293 cells.

BVRA KO HeLa cells stably expressing EKAREV-NLS were transfected with pPHFF, pCAGGS-PhyB-mCherry-HRas, and pCX4puro-PIF3-CRaf. Two days after transfection, the cells were imaged with epi-fluorescence microscopy. Timestamp shows time in minutes:seconds after first red light illumination.